

# SLOW MOTION Is Required for Within-Plant Auxin Homeostasis and Normal Timing of Lateral Organ Initiation at the Shoot Meristem in *Arabidopsis*

Daniel Lohmann,<sup>a,1,2</sup> Nicola Stacey,<sup>a,2</sup> Holger Breuninger,<sup>a</sup> Yusuke Jikumaru,<sup>b</sup> Dörte Müller,<sup>c</sup> Adrien Sicard,<sup>a</sup> Ottoline Leyser,<sup>c</sup> Shinjiro Yamaguchi,<sup>b</sup> and Michael Lenhard<sup>a,3</sup>

<sup>a</sup>Department of Cell and Developmental Biology, John Innes Centre, Norwich, NR4 7UH, United Kingdom

<sup>b</sup>RIKEN Plant Science Center, Tsurumi-ku, Yokohama City, Kanagawa, 230-0045, Japan

<sup>c</sup>Department of Biology, University of York, York, YO10 5YW, United Kingdom

The regular arrangement of leaves and flowers around a plant's stem is a fascinating expression of biological pattern formation. Based on current models, the spacing of lateral shoot organs is determined by transient local auxin maxima generated by polar auxin transport, with existing primordia draining auxin from their vicinity to restrict organ formation close by. It is unclear whether this mechanism encodes not only spatial information but also temporal information about the plastochron (i.e., the interval between the formation of successive primordia). Here, we identify the *Arabidopsis thaliana* F-box protein SLOW MOTION (SLOMO) as being required for a normal plastochron. SLOMO interacts genetically with components of polar auxin transport, and mutant shoot apices contain less free auxin. However, this reduced auxin level at the shoot apex is not due to increased polar auxin transport down the stem, suggesting that it results from reduced synthesis. Independently reducing the free auxin level in plants causes a similar lengthening of the plastochron as seen in *slo* mutants, suggesting that the reduced auxin level in *slo* mutant shoot apices delays the establishment of the next auxin maximum. SLOMO acts independently of other plastochron regulators, such as ALTERED MERISTEM PROGRAM1 or KLUH/CYP78A5. We propose that SLOMO contributes to auxin homeostasis in the shoot meristem, thus ensuring a normal rate of the formation of auxin maxima and organ initiation.

## INTRODUCTION

Leaves and flowers are initiated at the shoot apical meristem of higher plants in a defined spatial pattern and at regular time intervals (Steeves and Sussex, 1989). The spatial pattern of organ initiation determines the radial arrangement of organs around the stem, called phyllotaxis, while the interval between the initiation of two successive primordia, the so-called plastochron, influences the vertical spacing of organs on the mature stem. How the highly regular initiation of organs is regulated has long fascinated mathematicians and biologists alike, and different theoretical models have been put forward to explain this patterning (reviewed in Kuhlemeier, 2007).

Based on a large body of experimental work and mathematical modeling (Reinhardt et al., 2003; de Reuille et al., 2006; Jonsson et al., 2006; Smith et al., 2006b; Stoma et al., 2008; Bayer et al.,

2009), the current view is that localized maxima of the plant hormone auxin trigger organ initiation in the peripheral zone of the shoot meristem. These maxima are generated by coordinated polar auxin transport in the epidermis. The regular spacing of the maxima is achieved because initiating primordia transport auxin basally into the stem, thus depleting it from their immediate surroundings and inhibiting the initiation of primordia close by. As a result, the next primordium forms at a maximal distance from established organs. This auxin transport-based model is a representative of the wider class of inhibition-based phyllotactic models. At the cellular level, polar auxin transport is dependent on auxin efflux carriers of the PINFORMED (PIN) protein family (Okada et al., 1991; Galweiler et al., 1998), whose polar subcellular localization is regulated via reversible phosphorylation mediated by the protein kinase PINOID (PID) and protein phosphatases 2A (Friml et al., 2004; Michniewicz et al., 2007). Mutations in the founding member of the PIN family, *pin1*, as well as in *pid* result in a failure to initiate organs and as a consequence largely naked inflorescence stems (Okada et al., 1991; Christensen et al., 2000).

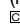
While the above concept and the different mathematical models based on it can explain most of the observations on the spatial patterning of organ initiation, how the temporal dynamics of organ formation are regulated remains unclear. In particular, a major unanswered question is whether the length of the plastochron merely emerges from the interaction between the growth patterns of the meristem and the dynamics of the

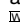
<sup>1</sup> Current address: Max-Planck-Institute of Molecular Cell Biology and Genetics, Pfotenhauerstrasse 108, 01307 Dresden, Germany.

<sup>2</sup> These authors contributed equally to this work.

<sup>3</sup> Address correspondence to michael.lenhard@bbsrc.ac.uk.

The author responsible for distribution of materials integral to the findings presented in this article in accordance with the policy described in the Instructions for Authors (www.plantcell.org) is: Michael Lenhard (michael.lenhard@bbsrc.ac.uk).

 Some figures in this article are displayed in color online but in black and white in the print edition.

 Online version contains Web-only data.

www.plantcell.org/cgi/doi/10.1105/tpc.109.071498

auxin-based inhibition mechanism or whether the plastochron is set by an independent cyclical regulatory system that acts as a biological clock, an idea first put forward by Hofmeister (1868). Numerical simulations and elegant physical experiments have demonstrated that inhibition-based mechanisms can generate all of the different types of phyllotaxis seen in nature, while a system based on Hofmeister's clock can produce opposite or spiral phyllotaxis (Douady and Couder, 1996; Smith et al., 2006a). Thus, although the assumption of an independently fixed plastochron may be too restrictive, there has been little experimental evidence that the auxin-based mechanism encodes not only spatial, but also temporal information.

Genetic studies in rice (*Oryza sativa*) and *Arabidopsis thaliana* have identified mutations in a number of genes that alter the

plastochron. In mutants for the rice *PLASTOCHRON1* (*PLA1*) and the homologous *Arabidopsis KLUH* (*KLU*)/*CYP78A5* gene, leaf formation is accelerated (Miyoshi et al., 2004; Wang et al., 2008). The same is seen in rice *plastochron2* mutants, and it has been suggested that these genes regulate the timing of leaf maturation, which would influence the strength of a hypothetical inhibitory signal emanating from young leaves to suppress organ initiation at the shoot meristem (Kawakatsu et al., 2006). Transcription factors of the SQUAMOSA-PROMOTER BINDING PROTEIN LIKE (SPL) family may represent this leaf-derived signal or be involved in its generation, as overexpressing SPL proteins in young organ primordia can lengthen the plastochron (Wang et al., 2008). *SPL* genes are under negative regulation by *microRNA156* (*miR156*), which promotes organ initiation at the

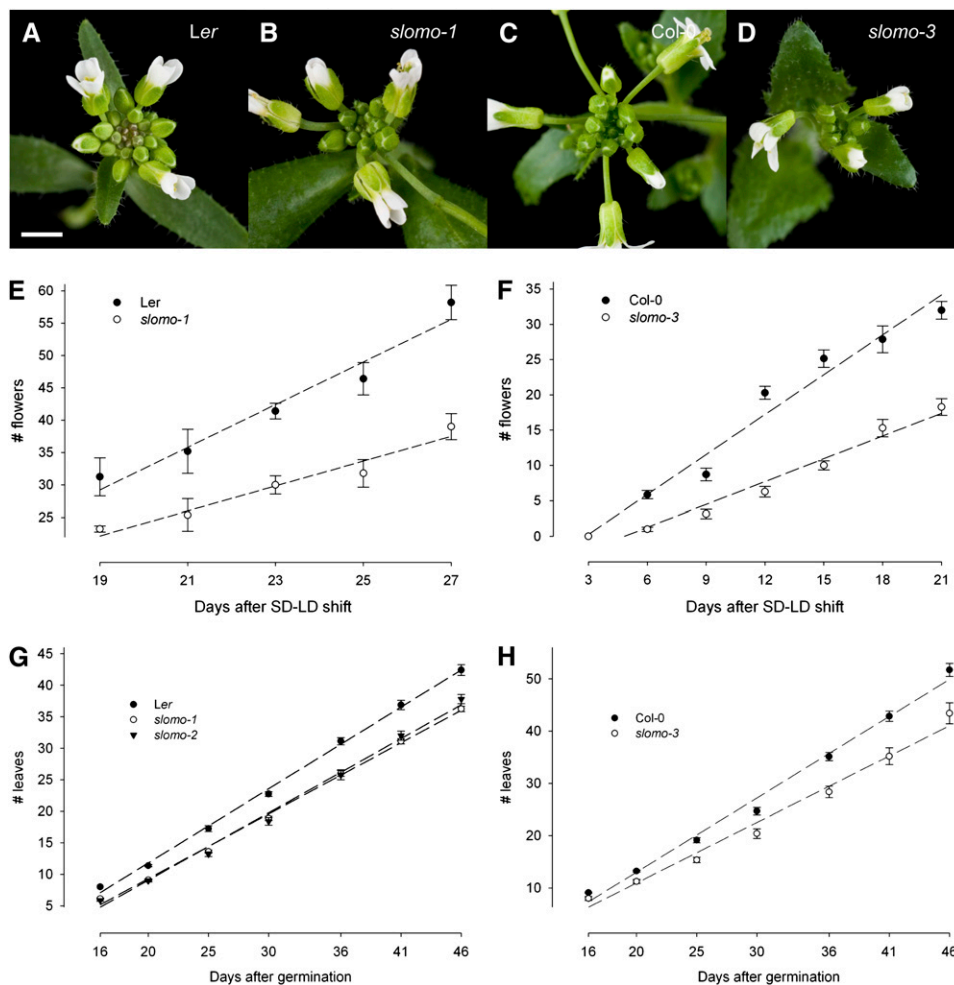


**Figure 1.** *slomo* Mutants Have a Lengthened Plastochron.

(A) to (D) Inflorescences of *Ler* wild type (A), *slomo-1* mutant (B), *Col-0* wild type (C), and *slomo-3* mutant (D).

(E) to (H) Quantification of the rate of flower (E,F) and leaf (G,H) initiation in *slomo* mutants compared with respective wild-type lines. To measure the rate of leaf initiation, plants were grown under short-day (SD) conditions. To measure flower initiation, synchronous flowering was induced by shifting plants from short days to long days (LD). Values for flower initiation in *slomo-2* are presented in Supplemental Figure 1E online.

Values are mean  $\pm$  SE from seven (E, F, and H) or five (G) plants. Dashed lines show linear regressions of organ number on time. Bar in (A) = 5 mm and applies to all four images.

[See online article for color version of this figure.]

shoot meristem by acting in young leaf primordia (Wang et al., 2008). A failure to properly express *miR156* is thought to underlie the lengthening of the plastochron in *serrate* mutants, affecting a protein required for processing of microRNAs (Grigg et al., 2005; Wang et al., 2008). Mutations in the *Arabidopsis* carboxypeptidase ALTERED MERISTEM PROGRAM1 (AMP1)/PRIMORDIA TIMING and its rice ortholog PLA3 shorten the plastochron (Chaudhury et al., 1993; Mordhorst et al., 1998; Kawakatsu et al., 2009), and this effect is associated with an enlarged shoot meristem and a higher cytokinin concentration (Helliwell et al., 2001; Kawakatsu et al., 2009). A link between cytokinin levels and the plastochron is also supported by the delay in organ formation observed in plants overexpressing cytokinin-catabolizing enzymes (Werner et al., 2001, 2003). However, despite the identification of these potential regulators, whether and how they interact with the auxin-based system that regulates primordia spacing is at present unclear.

Here, we describe the functional characterization of the novel *Arabidopsis* F-box protein SLOW MOTION (SLOMO), whose loss of function causes a specific lengthening of the plastochron, while maintaining a normal rate of cell production by the shoot meristem. We demonstrate that *slomo* mutants have a reduced level of free auxin in the shoot apex and provide independent evidence that reducing the auxin concentration slows down organ initiation. Thus, our findings suggest that the interplay between the auxin transport-based system and the growth patterns at the apex influences plastochron duration.

## RESULTS

### *slomo* Mutants Form Lateral Organs at a Reduced Rate

In an ethyl methanesulfonate (EMS) mutagenesis screen, we isolated two independent lines with a smaller inflorescence containing fewer flower buds and open flowers than Landsberg *erecta* (*Ler*) wild type (Figures 1A and 1B; see Supplemental Figures 1A and 1B online). Complementation tests showed these to be alleles of the same locus (see Supplemental Figure 1G online), which we termed *SLOMO*. After cloning the gene (see below), we also isolated a T-DNA insertion allele in the Columbia-0 (*Col-0*) background (Figures 1C and 1D; see Supplemental Figures 1C and 1D online).

The reduced number of developing flowers in the inflorescence suggested that *slomo* mutants have a longer plastochron and a reduced rate of lateral organ formation. To test this, we induced synchronous flowering by shifting plants from short to long days and counted the total number of developing flowers every 2 or 3 d by dissection. Indeed, the rate of organ formation by *slomo* mutant inflorescence meristems was significantly reduced (Figures 1E and 1F; see Supplemental Figure 1E online). To test whether this was also the case during the vegetative phase, we determined leaf numbers during growth in short days. Again, the rate of leaf formation was reduced in *slomo* mutants, albeit to a lesser extent than after the floral transition (Figures 1G and 1H). The effect in the vegetative phase is not only due to a delayed emergence of visible leaves, but reflects a reduced rate of initiation at the meristem, as *slomo-1* mutants grown in

short days form fewer leaves overall before flowering at the same time as the wild type (see Supplemental Figure 1F online). Thus, mutations in the *SLOMO* gene cause a lengthening of the plastochron in both the vegetative and the inflorescence meristem.

### *SLOMO* Encodes a Novel F-Box Protein with Widespread Expression

We isolated the *SLOMO* gene by positional cloning. Fine mapping and sequencing of mutant alleles identified G-to-A transitions typical of EMS-induced mutations in the *At4g33210* locus, predicted to encode a novel F-box protein with leucine-rich repeats (LRRs) (see Supplemental Figures 2A to 2D online). The *slomo-1* allele is due to a missense mutation of a highly conserved Gly to Glu in one of the C-terminal LRR domains; the *slomo-2* allele affects the conserved GT dinucleotide of the splice donor site of intron 9, causing missplicing with the retention of four additional nucleotides in the mRNA and a premature stop codon; and the *slomo-3* allele (Salk\_091125) harbors a T-DNA insertion in the first intron, which abolishes the production of full-length mRNA (see Supplemental Figures 2A to 2E and 3 online). As the *slomo-1* mutation generally showed the strongest phenotypes, we considered the possibility that it might represent

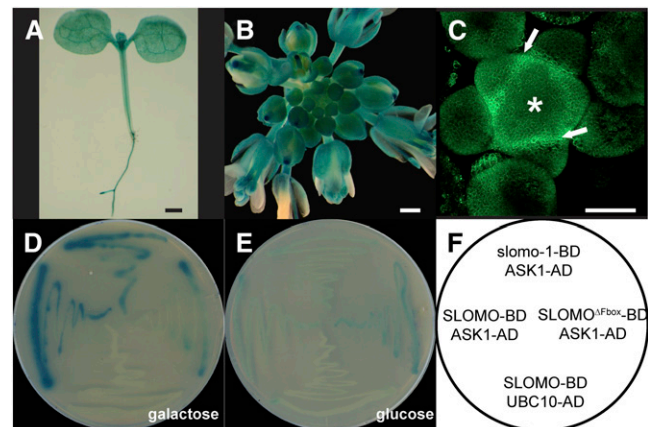


**Figure 2.** *SLOMO* Expression Pattern and Protein Interactions.

(A) and (B) GUS-stained seedling (A) and inflorescence (B) of a *ProSLOMO:GUS* reporter line. Promoter activity is visualized by the blue staining.

(C) Projection of a confocal z-stack through an inflorescence meristem of a *ProSLOMO::vYFP* expressing plant. Fluorescence is seen throughout the inflorescence meristem (asterisk) and surrounding flower primordia, with stronger expression at the boundaries between the two (arrows).

(D) to (F) Yeast two-hybrid interaction assay. Wild-type *SLOMO* protein and the form carrying the Gly-to-Glu mutation found in *slomo-1* interact with the *Arabidopsis* Skp1 homolog ASK1, as indicated by blue staining, but a version of *SLOMO* lacking the F-box (*SLOMO*<sup>ΔFbox</sup>) does not. UBC10 is an *Arabidopsis* E2 protein used as a negative control.

Bars = 1 mm in (A) and (B) and 50 μm in (C).

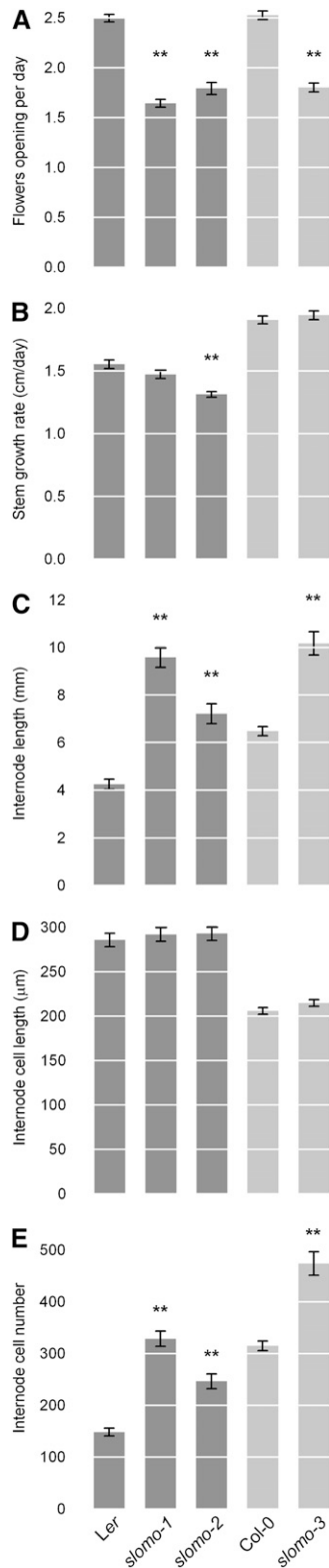


**Figure 3.** Shoot Growth and Lateral Organ Initiation Are Decoupled in *slomo* Mutants.

(A) to (E) Quantification of the indicated parameters in *slomo* mutants

a dominant-negative allele. However, the rate of flower formation in *slomo-1/+* heterozygous plants was not significantly reduced compared with the wild type (see Supplemental Figure 1H online), arguing against this possibility.

To determine the expression pattern of *SLOMO*, we analyzed lines carrying *ProSLOMO:β-glucuronidase (GUS)* and *ProSLOMO:vYFP<sub>er</sub>* reporter genes, vYFP<sub>er</sub> being an endoplasmic reticulum-localized form of VENUS-YFP. The respective constructs contain the same 5' genomic region as a fully complementing rescue construct (see Supplemental Figure 2F online), suggesting they harbor all *cis*-elements essential for *SLOMO* function. GUS activity in the *ProSLOMO:GUS* line was observed throughout the entire seedling (Figure 2A) and in all of the inflorescence except for old petals (Figure 2B). Confocal microscopy on the *ProSLOMO:vYFP<sub>er</sub>* line indicated expression throughout the inflorescence meristem and flower meristems, with higher levels at the boundary between the inflorescence meristem and initiating flower primordia (Figure 2C). Thus, the *SLOMO* promoter shows widespread activity in vegetative and flowering plants.

F-box proteins generally act as the specificity-determining components of multiprotein E3 ubiquitin-ligases, so-called SCF complexes. The F-box interacts with the suppressor of kinetochore protein 1 (Skp1p) protein or its homologs in the SCF complex, while other domain(s) in the F-box protein are responsible for recruiting specific substrates for ubiquitination. Using a yeast two-hybrid interaction assay, we found that the *SLOMO* protein interacts with the protein encoded by the *ARABIDOPSIS SKP1 HOMOLOG1* gene (*ASK1*; Figures 2D to 2F). This interaction is largely abolished by deletion of the F-box but is unaffected by the missense mutation found in the *slomo-1* allele. This suggests that the *SLOMO* protein acts as the F-box component of an *Arabidopsis* SCF complex.

The F-box and LRR-containing regions of the *SLOMO* protein are strongly conserved throughout higher plants; by contrast, the N-terminal region preceding the F-box is much more divergent (see Supplemental Figure 3 online).

### The Plastochron Defect in *slomo* Mutants Reflects a Decoupling of Shoot Growth and Organ Initiation

The reduced rate of organ formation by *slomo* mutant shoot meristems could result from a specific requirement for *SLOMO* function in organ initiation or from a more pleiotropic role in promoting general shoot meristem activity. To determine the extent of pleiotropy in the effects of *slomo* loss of function, we measured the rate of overall shoot growth and the length

compared with their respective wild-type lines.

(A) Flowers opening per day.

(B) Rate of shoot growth.

(C) Mature internode length.

(D) Epidermal cell length in mature internodes.

(E) Number of epidermal cells per cell file in mature internodes, as calculated from (C) and (D).

Values are mean  $\pm$  SE from 20 (A) and (B) or 15 (C) plants per genotype and from at least 180 cells from 10 plants per genotype (D) and (E).

\*\*P < 0.01 compared with the respective wild type by Student's *t* test.

and constituent cell number of mature internodes as an approximation for overall meristem activity. We first confirmed the lengthened plastochron in the inflorescence of *slomo* mutants using the number of flowers opening up per day as a nondestructive measure (Figure 3A). Except for *slomo-2* mutants, which have a slightly reduced rate of overall shoot growth, the shoot of plants carrying either of the other two mutant alleles elongates as rapidly as that of the control plants (Figure 3B). Conversely, mature internodes of all three *slomo* mutant alleles are significantly longer than in the wild type (Figure 3C) and consist of an increased number of cells with wild-type length (Figures 3D and 3E). Most of the proliferative divisions that generate the cells of the mature internode occur in the subapical region; assuming that the extent of this subapical cell proliferation is not affected by *SLOMO*, the increased internode length suggests that in *slomo* meristems more cells are allocated to the internodes for each successive organ formed. Consistent with this interpretation, the plastochron ratio (i.e., the ratio of the distances of successive flower primordia to the meristem center) (Richards, 1951) tends to be higher in *slomo* mutants than in the wild type (Table 1, Figures 4A and 4B), suggesting that the meristem grows more between the initiation of successive organs. By contrast, the divergence angle between successive primordia was unchanged, confirming that *SLOMO* does not affect phyllotaxis (Table 1, Figures 4A and 4B). Thus, these measurements strongly suggest that the lengthened plastochron in *slomo* mutants reflects a specific delay in the initiation of lateral organs at the shoot meristem, rather than a generalized reduction in meristem activity.

### The Lengthened Plastochron in *slomo* Mutants Is Not Due to Altered Shoot Meristem Dimensions or Division Activity

To determine meristem activity in *slomo* mutants more directly, we measured the dimensions of the inflorescence meristem and its division activity from *slomo-1* and *slomo-3* mutants compared with the wild type. Using scanning electron microscopy (*slomo-1*) or histological sections (*slomo-3*), both mutant alleles were found to have inflorescence meristems that are <10% smaller than the respective wild-type plants (Figures 4A to 4D, Table 1). We used *in situ* hybridization against *CLAVATA3* mRNA to determine the relative sizes of central and peripheral zones in the meristem (Figures 4E and 4F). *CLV3* is specifically expressed in the stem cells of the meristem within the central zone and encodes a secreted peptide that limits the number of stem cells (Fletcher et al., 1999; Lenhard and Laux, 2003). In this experiment, there was only a marginal difference in overall meristem size between Col-0 wild-type and *slomo-3* mutant plants (Table 1). The number of *CLV3*-expressing cells and, thus, the size of the central zone was indistinguishable between the two genotypes, suggesting that zonation of the meristem is not affected by loss of *SLOMO* function.

Is the small difference in overall meristem size enough to explain the observed reduction in the rate of flower formation? To test this, we measured the rate of flower formation in plants that have a >20% smaller, yet still self-maintaining meristem due to an increased copy number of *CLAVATA3* (*CLV3*) (Figure 4G) (Lenhard and Laux, 2003). Despite a much larger reduction in

**Table 1.** Quantification of Meristem Parameters in Wild-Type and *slomo* Mutant Plants

	<i>Ler</i>	<i>slomo-1</i>	Col-0	<i>slomo-3</i>
Inflorescence meristem size ( $\mu\text{m}$ )				
Mean	79.2	73.7*	95.9/105.4	86.4*/100.1
SE	1.6	1.1	2.7/3.6	2.9/4.2
<i>n</i>	10	10	8/15	9/11
S-phase index (%)				
Mean	6.1	5.4	17.4	16.6
SE	0.51	0.63	0.56	0.84
<i>n</i>	13	10	18	16
<i>CLV3</i> -expressing cells				
Mean			15.4	14.5
SE			0.6	1.0
<i>n</i>			15	11
Divergence angle ( $^{\circ}$ )				
Mean	136.8	135.9	137.7	137.3
SE	1.80	2.0	0.31	0.32
<i>n</i>	11	13	12	9
Plastochron ratio				
Mean	1.140	1.166*	1.098	1.114
SE	0.007	0.006	0.007	0.003
<i>n</i>	11	13	12	9

For inflorescence size, values for *Ler* and *slomo-1* were obtained from scanning electron micrographs. For Col-0 and *slomo-3*, the values represent the corresponding measurement from tissue sections, with the first values obtained from the *histone H4 in situ* hybridization, and the second values obtained from the *CLV3 in situ* hybridization, respectively. Asterisks indicate significant difference from the respective wild type at  $P < 0.05$ . The S-phase index is the proportion of *histone H4*-expressing cells of all the cells in a longitudinal section of the meristem. The difference in absolute values for the S-phase index between genotypes in the *Ler* and Col-0 backgrounds is likely due to the latter having been harvested very shortly after the floral transition, while the former represent older inflorescence meristems. Cell division activity is known to be higher in meristems at the floral transition than in established inflorescence meristems (Geier et al., 2008).

meristem size in the *CLV3*-overexpressing plants, their rate of flower formation was only moderately decreased (Figure 4G), suggesting that the lengthened plastochron in *slomo* mutants cannot be explained by the slight reduction in meristem size. As for cell division activity, there was no significant difference between mutant and wild-type meristems (Table 1), consistent with the apparently normal output of shoot epidermal cells by mutant meristems (Figures 3B to 3E). Together, these observations support the above conclusion that the *SLOMO* gene specifically affects the initiation of lateral organs at the meristem, rather than influencing the plastochron indirectly via more general effects on meristem architecture or function.

### *slomo* Mutant Shoot Apices Contain Reduced Auxin Levels

The localized auxin maxima that trigger organ initiation are the result of coordinated polar auxin transport via the PIN1 auxin efflux carrier, whose intracellular polarity is determined by phosphorylation via the PID protein kinase. Thus, it is conceivable that wild-type *SLOMO* activity promotes organ initiation in one of at

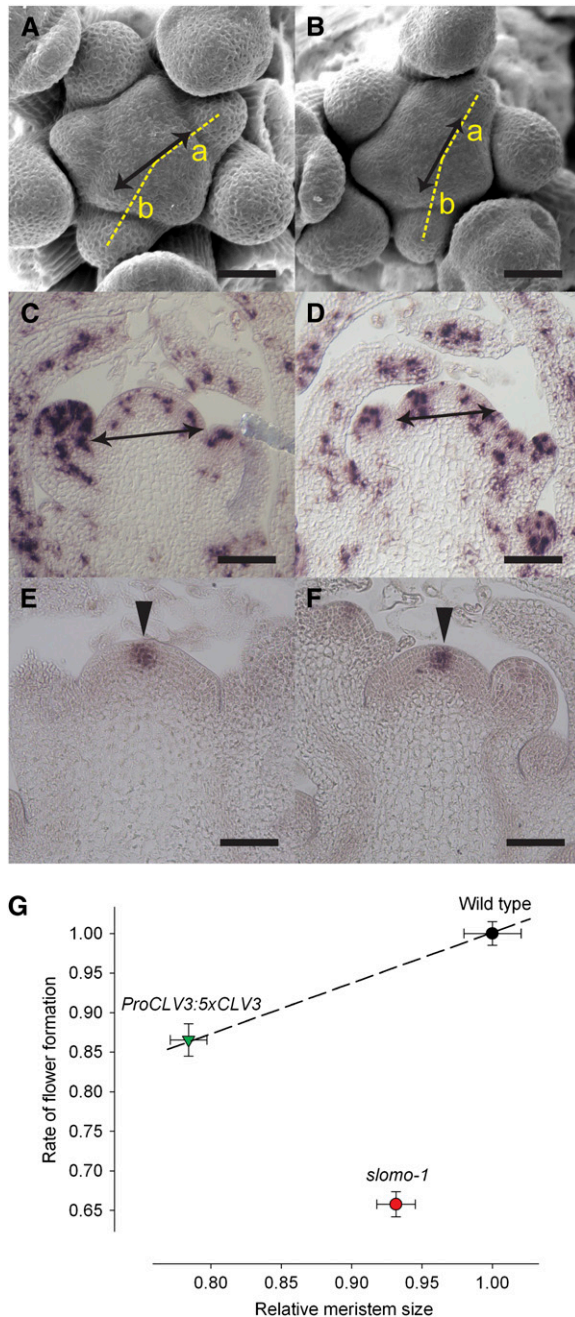


**Figure 4.** Measurements of Meristem Dimensions and Cell Division Activity.

**(A)** and **(B)** Scanning electron micrographs of dissected inflorescence meristems of *Ler* wild-type **(A)** and *slomo-1* mutant plants **(B)**. Arrows indicate where the measurements of meristem size were taken, from the youngest visible flower primordium to the furrow separating the inflorescence meristem and the flower initiated four plastochrons earlier. The dashed yellow lines indicate the distances from the center of the inflorescence meristem to the centers of two successive flower meristems used for calculating the plastochron ratio  $b:a$ .

**(C)** to **(F)** In situ hybridizations using a histone H4 **(C)** and **(D)** or a *CLV3* **(E)** and **(F)** antisense riboprobe on longitudinal sections through Col-0

at least three ways: *SLOMO* could act in auxin perception, allowing cells to respond efficiently to the new auxin maximum; it could promote polar auxin transport, contributing to a timely establishment of the next auxin maximum; or it could increase the overall amount of auxin available at the shoot meristem, ensuring there is sufficient auxin for the polar transport machinery to form the next maximum at the normal rate.

To test for a general role of *SLOMO* in auxin perception, we quantified the effects of exogenously added auxin on root growth. Root growth was inhibited indistinguishably in *slomo* mutant and wild-type plants by increasing auxin concentrations (see Supplemental Figure 4A online). Also, at the inflorescence meristem, no difference was detectable in the expression pattern and strength of the synthetic auxin-response reporter *ProDR5:VENUS* (see Supplemental Figure 5 online). These results suggest that auxin perception is not grossly affected in *slomo* mutants.

To test for an involvement of *SLOMO* in polar auxin transport, we generated double mutants of *slomo* and *pid* or *pin1*. Single mutants of *pid* or *pin1* form very few aberrant flowers, before the inflorescence meristem terminates in a naked pin (Figure 5A). Assuming that the prolonged plastochron in *slomo* mutants results from impaired polar auxin transport, one would either expect epistasis of *pid* or *pin1* over *slomo*, if *SLOMO* acts in the same pathway as these two; or an enhanced *pin1*-like phenotype in the double mutants, if *SLOMO* influences polar auxin transport independently from *PID* and *PIN1*. In contrast with either prediction, combining the *slomo-1* mutation with either a strong (*pid-1*) or an intermediate (*pid-2*) mutant allele of *PID* caused a significant increase in the number of flowers formed before the meristem transitioned to a naked pin (Figures 5A, 5B, and 5G). This partial rescue of organ formation was not specific to double mutants involving *pid* alleles but was similarly observed in *pin1 slomo-1* mutants (Figure 5H); neither was the rescue due specifically to the *slomo-1* allele, as *pin1 slomo-3* mutants also formed an increased number of flowers before the pin (Figure 5H). The latter plants also showed additional phenotypes not observed in *pin1* single mutants, such as collar-like cauline leaves encircling the inflorescence stem or wing-like leaves emanating from a long stretch of the stem (Figures 5C to 5F), indicating an increased, albeit improperly patterned ability to form lateral organs. Thus, the loss of *SLOMO* function in backgrounds with compromised

wild-type **(C)** and **(E)** and *slomo-3* mutant **(D)** and **(F)** inflorescence meristems. Arrows in **(C)** and **(D)** indicate where the measurements of meristem size were taken between the furrows separating the youngest visible flower primordia in the sections. Arrowheads in **(E)** and **(F)** indicate the domain of *CLV3* expression in the central zone of the meristem.

**(G)** Relationship between relative meristem size and the relative rate of flower formation in the indicated genotypes. Data for meristem size of the *CLV3*-overexpressing and respective wild-type plants are from Lenhard and Laux (2003). The dashed line shows the predicted dependence of the rate of organ initiation on meristem size based on the *CLV3*-overexpressing plants. Values are mean  $\pm$  SE from at least 12 plants per genotype, taken from Figure 3A, Table 1, and Lenhard and Laux (2003).

Bars = 50  $\mu$ m in **(A)** to **(F)**.

[See online article for color version of this figure.]

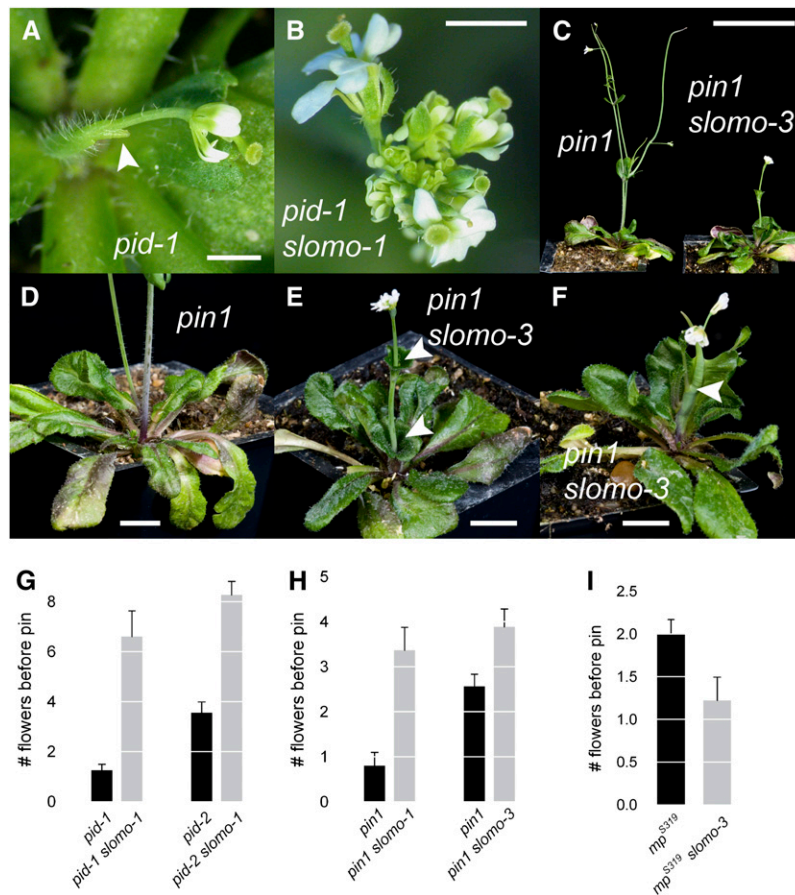


**Figure 5.** Interactions of *slomo* Mutations with the Polar Auxin Transport System.

(A) to (F) Light micrographs.

(A) In *pid-1* single mutants, organ formation at the inflorescence meristem terminates after the initiation of one or two flowers, giving rise to a naked pin (arrowhead).

(B) By contrast, *pid-1 slomo-1* double mutants form many more flowers before transition of the meristem to a naked pin (not visible).

(C) Whole-plant phenotype of *pin1* single and *pin1 slomo-3* double mutants.

(D) and (E) Close-ups of the inflorescence stem of the two plants shown in (C). *pin1 slomo-3* double mutants form collar-like cauline leaves encircling the inflorescence stem (arrowheads in [E]), which are never observed in *pin1* single mutants (D) under our growth conditions.

(F) A *pin1 slomo-3* double mutant showing extensive fusion of cauline leaves with the inflorescence stem (arrowhead).

(G) to (I) Quantification of flower formation before the meristem transits to a naked pin in the indicated genotypes. Values are mean  $\pm$  SE from at least nine plants per genotype (except for *pid-1* with only four plants). All differences are statistically significant at  $P < 0.01$  ([G] and [H]) or  $P < 0.05$  (I).

Bars = 4 mm in (A) and (B), 5 cm in (C), and 1 cm in (D) to (F).

[See online article for color version of this figure.]

polar auxin transport can partially rescue the formation of lateral organs at the shoot meristem. To test whether this effect was specific for mutations affecting polar auxin transport, we eliminated *SLOMO* function in a *monopteros* (*mp*) mutant background. *MP* encodes AUXIN RESPONSE FACTOR5 that regulates gene expression in response to auxin perception (Hardtke and Berleth, 1998). Plants carrying the weak *mp<sup>S319</sup>* allele form on average two flowers, before the meristem terminates in a naked pin (Figure 5I) (Cole et al., 2009). Double mutants of *mp<sup>S319</sup>* and *slomo-3* form even fewer flowers (Figure 5I). This indicates that loss of *SLOMO* function specifically alleviates the phenotype of mutants affecting polar auxin transport, but not auxin signal-

ing, and suggests that polar auxin transport is not less efficient in *slomo* mutants.

To test the third possible auxin-related role of *SLOMO* in stimulating organ initiation (i.e., the promotion of high auxin levels at the shoot meristem), we measured the concentration of free indole-3-acetic acid (IAA) as the main active auxin in dissected inflorescence apices of wild-type and *slomo* plants. Both mutant alleles analyzed had only half the wild-type amount of IAA in the apex (Figure 6A). This finding contrasts with additional aspects of the *slomo* mutant phenotype, such as longer hypocotyls (see Supplemental Figure 4C online), a slightly reduced branching (see Supplemental Figures 1A to 1D online) and enhanced

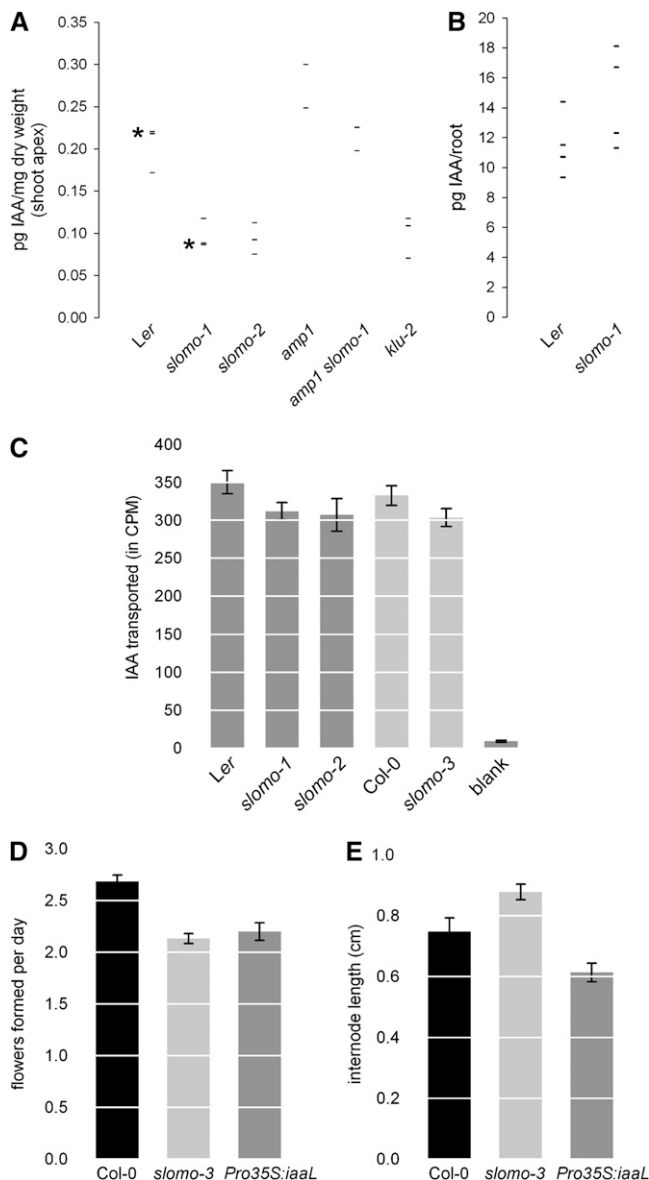


**Figure 6.** *slomo* Mutant Shoot Apices Have a Reduced Amount of Free Auxin.

(A) and (B) Free IAA levels in dissected inflorescence meristems (A) or in roots (B) of the indicated genotypes. Each mark represents a measurement on an independent pooled sample of 20 apices or roots, respectively. For *amp1* and *amp1 slomo-1*, only two replicates were analyzed. For clarity, the asterisks in (A) each mark two independent, very similar measurements. The roots were collected 7 d after germination to reduce the morphological differences between *slomo-1* and wild-type roots that develop later due to the former's increased lateral root formation (cf. Supplemental Figure 4B online).

(C) Quantification of bulk polar IAA transport in stem segments of the indicated genotypes. Mean values  $\pm$  SE of radiolabel transported (in cpm) are shown. There is no significant difference between either wild type and the respective mutant alleles. At least 19 stem segments were assayed per genotype.

(D) and (E) Quantification of the rate of flower formation (D) and mature internode length (E) in the indicated genotypes. Values are mean  $\pm$  SE

formation of lateral roots (see Supplemental Figure 4B online), all of which are consistent with a higher, rather than a lower auxin level throughout the rest of the plant. Indeed, measuring free IAA in roots indicated that *slomo* mutants tend to have slightly higher auxin levels in roots (Figure 6B), consistent with the enhanced lateral root formation (see Supplemental Figure 4B online). Thus, *SLOMO* is required for normal auxin distribution within the plant.

### The Reduced Auxin Levels in *slomo* Mutant Apices Are Not Due to Increased Polar Transport Down the Stem

The partial rescue of organ formation in polar auxin transport mutants by loss of *SLOMO* function and the reduced level of free auxin in *slomo* mutant shoot apices raised the possibility that the *slomo* mutations lead to increased polar auxin transport down the stem, partially draining the shoot apex of auxin. To test this possibility, we measured polar transport of radioactively labeled IAA through segments of the inflorescence stem in wild-type and *slomo* mutant plants. There was no significant difference between rates of transport between the wild type and mutants (Figure 6C). This indicates that the reduced levels of free auxin in the mutant apices are not due to increased polar transport, but rather that they may result from reduced auxin synthesis at the mutant apices.

### Reducing IAA Levels Lengthens the Plastochron

To determine whether the reduced auxin levels in *slomo* mutant apices could be causal for the lengthening of the plastochron, we measured the rate of flower formation in plants overexpressing the bacterial *iaaL* protein (Jensen et al., 1998). *iaaL* conjugates IAA to Lys and thus leads to lower levels of active free auxin throughout the plant. Indeed, *Pro35S:iaaL*-expressing plants had a similarly reduced rate of flower formation as *slomo* mutants (Figure 6D). Other aspects of the phenotype were different, however, with *Pro35S:iaaL* plants forming shorter internodes (Figure 6E) and having a reduced apical dominance (Jensen et al., 1998), which are likely to reflect the strongly reduced auxin levels throughout all of the plant resulting from the ubiquitous conjugation of IAA.

### Genetic Interactions of *slomo* with Other Plastochron Mutants

Several plant lines have been described that have a faster rate of organ initiation, such as *klu* and *amp1* mutants or *miR156*-overexpressing plants (Chaudhury et al., 1993; Mordhorst et al., 1998; Schwab et al., 2005; Wang et al., 2008). To test whether *SLOMO* genetically interacts with any of these, we analyzed the rate of flower formation in the respective double mutants. Plants overexpressing *miR156b* did not show an accelerated formation of flowers under our growth conditions, and the plastochron in the inflorescence of *Pro35S:miR156b; slomo-3* plants was

from 10 plants per genotype. Mean values for *slomo-3* and *Pro35S:iaaL* are significantly different from Col-0 at  $P < 0.001$  (D) and  $P < 0.05$  (E) when compared using a *t* test with Bonferroni correction.



indistinguishable from that in *slomo-3* single mutants (see Supplemental Figure 6E online). Also, the overall architecture of *Pro35S:miR156b; slomo-3* plants was intermediate between that of the parental lines (see Supplemental Figures 6A to 6D online), indicating an independent function of *SLOMO* and *miR156*.

*klu-2 slomo-1* double mutants showed an intermediate phenotype, with a reduction in the rate of organ formation compared with the *klu-2* single mutant (Figure 7). By contrast, the *amp1* mutation was epistatic over the *slomo-1* phenotype, with double mutants forming flowers at the same increased rate as *amp1* single mutants (Figure 7). This is consistent with both genes acting in a common pathway.

To further explore the function of *AMP1* and *KLU* in plastochron regulation, we analyzed double mutants between these genes and *pid-2*. In both cases, the number of flowers formed before the meristem transitioned to a naked pin was increased in the double mutants (Figures 8A, 8B, 8E to 8G, and 8I). Conversely, overexpression of *KLU* in its endogenous expression domain (Anastasiou et al., 2007) in a *pid-2* mutant background reduced the number of flowers formed before the pin (Figures 8C, 8D, 8G, and 8H). Thus, in contrast with the opposite single mutant phenotypes in *amp1* and *klu-2* compared with *slomo*, when combined with *pid* mutations they produce the same effect, arguing against *SLOMO* acting in a common genetic pathway with either *AMP1* or *KLU*.

To address the basis for the altered plastochron in *amp1* and *klu-2* mutants, we measured the level of free IAA in dissected shoot apices (Figure 6A). *klu-2* mutant apices contained only half the wild-type level of IAA. By contrast, in *amp1* mutants, the auxin content was increased by ~25% compared with the wild type, and *amp1 slomo-1* double mutant apices had approximately wild-type IAA levels. This indicates firstly that the auxin level is not always directly related to the rate of organ formation; secondly, the limited effect of the *slomo* mutation on auxin levels in an *amp1* mutant background indicates that *SLOMO* is still at least partly active in *amp1* mutants.

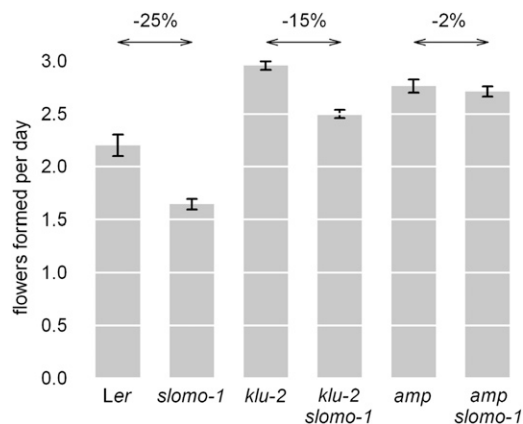


**Figure 7.** Double Mutant Analysis.

Rate of flower formation in plants of the indicated genotypes. Percentages show the changes in the rate of flower formation due to loss of *SLOMO* function in the respective backgrounds. Values are mean  $\pm$  SE from at least nine plants per genotype.

## DISCUSSION

### *SLOMO* Function Is Specifically Required for a Normal Rate of Organ Initiation by the Shoot Meristem

The spatial patterning of lateral organ initiation at the shoot meristem has been intensively studied and shown to involve transient auxin maxima that determine the position of the next organ (Reinhardt et al., 2003; de Reuille et al., 2006; Jonsson et al., 2006; Smith et al., 2006b; Stoma et al., 2008; Bayer et al., 2009). By contrast, much less is known about the timing of organ initiation. For example, it is unclear whether this timing merely emerges from the interaction between the dynamics of the auxin transport system and growth patterns at the shoot meristem or whether the plastochron is set by an independent regulatory system, acting as a biological clock.

Here, we identify the novel *Arabidopsis* F-box protein *SLOMO* as being required for normal plastochron timing. Mutations in *SLOMO* result in a specific delay in the initiation of lateral organs, with minimal pleiotropic effects on other aspects of shoot meristem function. This is based on our result that *slomo* mutant shoot meristems appear to form cells at a largely wild-type rate, as judged both from the overall growth behavior and increased internode length of the shoot, as well as from direct measurements of meristem dimensions and mitotic activity. This situation is in contrast with other cases of a lengthened plastochron, for example, that resulting from the reduced cytokinin levels in tobacco (*Nicotiana tabacum*) plants overexpressing cytokinin oxidase (Werner et al., 2001). In these cytokinin-deficient plants, the reduced rate of leaf formation was due to an overall decrease in cell production by the shoot meristem, which was much smaller than in the wild type. Thus, wild-type *SLOMO* function appears to be specifically required to ensure normal plastochron duration.

### *SLOMO* and within-Plant Auxin Distribution

A critical question concerns the primary defect in *slomo* mutants. Based on our measurements of IAA levels, *SLOMO* appears to be required to maintain the appropriate distribution of auxin levels within the plant. Loss of *SLOMO* function reduces the level of free IAA at the shoot apex, while no such reduction is observed in roots. If anything, several additional phenotypes of *slomo* mutants are consistent with slightly increased auxin levels in other parts of the plant, such as the longer hypocotyls and the higher density of lateral roots. These apparent changes in the within-plant distribution of auxin could result from an alteration in the spatial pattern of auxin biosynthesis or in auxin transport. In either case, the previously described feedback regulation over auxin synthesis (Ljung et al., 2001) appears compromised as well, resulting in a reduced steady state level of auxin in the meristem. Our double mutant analyses of *slomo* and mutations affecting polar auxin transport had suggested a possible role for *SLOMO* in auxin transport. Loss of *SLOMO* function in a *pid* or *pin1* mutant background defective in polar auxin transport partially rescued organ formation, while combining *slomo* and a weak *mp* mutation defective in auxin perception caused, if anything, a more severe mutant phenotype with fewer flowers

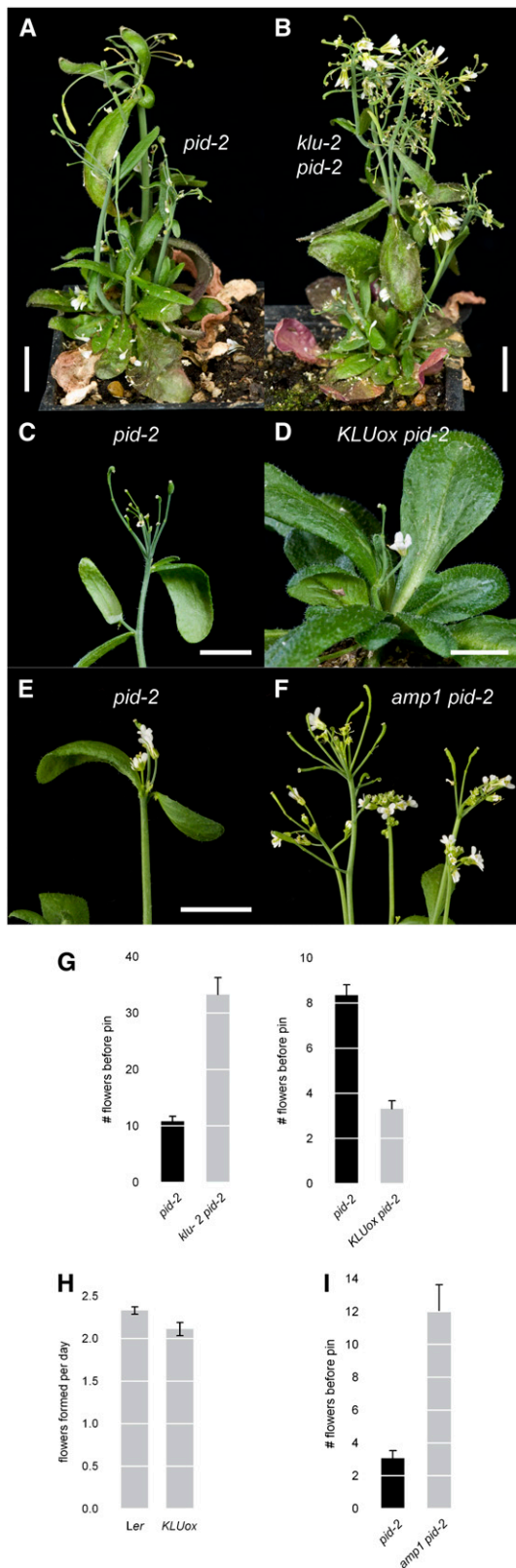


**Figure 8.** Genetic Interactions of *KLU* and *AMP1* with Polar Auxin Transport Mutants.

being initiated by the inflorescence meristem before transition to a naked pin. However, directly measuring the ability of *slo* mutant stems to transport auxin basipetally indicated no difference from the wild type. Thus, together with the reduced amount of auxin in the mutant shoot apices, this result suggests that *SLOMO* functions to promote auxin biosynthesis at the shoot apex. Understanding how a mutation that reduced the level of free IAA at the shoot apex can specifically promote flower formation when polar auxin transport is compromised is an important question for future study.

#### Auxin Levels and the Plastochron

What causes the lengthening of the plastochron in *slo* mutants? We have tested three possibilities suggested by the current auxin transport–based models of lateral organ initiation (i.e., a defect in auxin perception or in polar auxin transport or a reduction in the auxin levels available at the shoot meristem). Our results indicate that there is no gross defect in auxin perception or in polar auxin transport. There is, however, a strong reduction in free IAA levels at the shoot apex to only half the wild-type value. When auxin levels are independently reduced by the overexpression of a catabolizing enzyme, the plastochron is similarly lengthened as in *slo* mutants, supporting the notion that the auxin deficiency in the *slo* meristem causes the delay in organ initiation. In this view, it would take longer to build up the next local concentration maximum from a reduced overall level of free auxin to trigger initiation of a new organ. One important implication of this hypothesis concerns the way in which auxin maxima are perceived in the meristem. Based on studies in maize (*Zea mays*) *aberrant phyllotaxy1* mutants, it has recently been proposed that organ initiation requires the formation of a relative auxin maximum compared with the background level in surrounding cells (Lee et al., 2009). However, if auxin concentration was only measured relative to neighboring cells, the

(A) to (F) Light micrographs.

(A) and (B) Whole-plant phenotypes of *pid-2* single (A) and *pid-2 klu-2* double mutants (B). Note the increased number of flowers formed in the double mutant.

(C) and (D) Overexpression of *KLU* in a *pid-2* mutant background (D) reduces the number of flowers formed compared with *pid-2* single mutants (C).

(E) and (F) Loss of *amp1* function in a *pid-2* mutant background (F) allows for the formation of more flowers before transition of the meristem to a naked pin than in *pid-2* single mutants.

(G) Quantification of flower formation before the meristem transits to a naked pin in the indicated genotypes.

(H) Quantification of the rate of flower formation in the Ler wild type versus plants overexpressing *KLU* in the endogenous expression domain (*KLUox*) (Anastasiou et al., 2007).

(I) Quantification of flower formation before the meristem transits to a naked pin in the indicated genotypes.

Values are mean  $\pm$  SE from at least seven (G) or nine (H) and (I) plants per genotype. All differences are significant at  $P < 0.05$  (H) or  $P < 0.01$  (G) and (I), when compared using Student's *t* test.

Bars = 1 cm.

[See online article for color version of this figure.]

absolute overall auxin level would not be expected to have a strong influence on the timing of maxima perception. Thus, the above hypothesis implies that an absolute concentration threshold of auxin has to be exceeded locally to trigger initiation of a new organ, which would take longer to reach when starting from a lower overall level.

There are two possible objections to our hypothesis. First, there is potentially a circular relationship between auxin levels and organ formation, as young organs appear to be the major source of IAA synthesis in the shoot (Ljung et al., 2001). Thus, if *slomo* mutations lengthened the plastochron independently of auxin, the reduced number of young primordia surrounding the meristem at any time could in itself cause lower auxin levels. Second, *klu* mutants form flowers at an increased rate despite similarly low auxin levels in the shoot meristem as *slomo* mutants, indicating that at least one of the two genes influences the plastochron independently of auxin. At present, we cannot formally rule out that auxin levels in *slomo* mutant apices are lower because of an independent lengthening of the plastochron; however, the reduced rate of organ formation in *iaaL*-overexpressing plants demonstrates that the causality we propose is plausible. Also, as the function of *KLU* is independent of *SLOMO* based on our genetic analysis, we favor the above hypothesis that the effect of *SLOMO* on the plastochron is mediated by its effect on auxin levels in the meristem, while the shortening of the plastochron in *klu* mutants may mainly result from faster cell cycling (Wang et al., 2008).

### Roles of *KLU* and *AMP1* in Regulating Organ Initiation at the Meristem

*SLOMO* acts independently of two other known plastochron regulators, *miR156* and *KLU*. The interaction between *SLOMO* and *AMP1* is more complex. Mutation of *amp1* is epistatic over *slomo* at the level of the plastochron phenotype. By contrast, loss of *SLOMO* function still causes a slight reduction in auxin levels in an *amp1* mutant background, indicating that *SLOMO* remains at least partially active in the absence of *AMP1* function. Also, *pid-2 amp1* double mutants show a similarly increased flower formation as *pid-2 slomo* double mutants, despite the opposite single mutant phenotypes of *amp1* and *slomo*. Therefore, we favor the hypothesis that *SLOMO* and *AMP1* act in largely independent pathways. The observed epistasis in terms of the plastochron may be linked to the enlargement of the shoot meristem due to loss of *AMP1* function (Helliwell et al., 2001).

How do *KLU* and *AMP1* regulate the plastochron? In *klu* mutants, the plastochron is shortened despite a reduction in auxin levels to the same extent as in *slomo*. Although *amp1* mutant meristems contain more auxin than the wild type, the auxin level in *amp1 slomo* double mutant meristems is the same as in the wild type, and yet organ formation in the double mutants is still faster. Both *amp1* and *klu* mutations also largely rescue organ formation by *pid* mutant meristems. By contrast, *KLU* overexpression suppresses flower initiation in *pid* mutants. This is consistent with the idea that *AMP1* and *KLU* contribute to the active suppression of organ initiation, possibly by delaying organ maturation and allowing increased production of an inhibitor emanating from young organs, as proposed for *PLA* genes from

rice (Kawakatsu et al., 2009). When this suppression is relieved in the mutants, organs form faster despite the same (*amp1 slomo*) or lower (*klu*) auxin levels than in the wild type. One possibility would be that in *amp1* and *klu* mutants, the value of the auxin threshold level, at which a new primordium is initiated, is reduced. Also, cell division is accelerated in *pla3* and *klu* mutants (Wang et al., 2008; Kawakatsu et al., 2009), which is likely to also contribute to the faster organ initiation.

In summary, we have identified a specific role for the *SLOMO* F-box protein in regulating the rate of lateral organ initiation at the shoot meristem. Our characterization of *SLOMO* function has generated several testable hypotheses about the role of the polar auxin transport-based system in determining the plastochron. Whether and how other regulatory pathways, exemplified by *AMP1* and *KLU*, interact with the auxin transport-based system or function independently in plastochron regulation are further important questions for future studies.

## METHODS

### Plant Lines and Growth Conditions

The *slomo-1* and *slomo-2* alleles were isolated from an EMS mutagenesis screen in the *bb-1* background. Before analysis, both mutants were backcrossed three times to the *Ler* wild type. The *slomo-3* allele in the Col-0 background was isolated from the SALK collection of T-DNA insertion lines (SALK\_091125). *klu-2*, *pid-1*, *pid-2*, *mp<sup>S319</sup>*, *Pro35S:miR156b*, and *Pro35S:iaaL* seeds have been described before (Jensen et al., 1998; Christensen et al., 2000; Schwab et al., 2005; Anastasiou et al., 2007; Cole et al., 2009). *pin1* (Gabi-KAT line GK\_051A10) was provided by Klaus Palme. *amp1/pt* mutants were obtained from the Nottingham Arabidopsis Stock Centre (stock ID N235).

Unless stated otherwise, plants were grown under long-day conditions (16 h light/8 h dark) at 20°C with a light intensity of 120  $\mu\text{mol photons m}^{-2} \text{s}^{-1}$ . For measuring leaf numbers, plants were grown under short-day conditions (9 h light/15 h dark) at 20°C with a light intensity of 120  $\mu\text{mol photons m}^{-2} \text{s}^{-1}$ .

### Plastochron and Internode Measurements

For direct measurements of the plastochron, plants were grown in short days for 30 d, before shifting to long days to induce synchronous flowering. At the indicated times after the shift, the plants were dissected under a stereomicroscope, and the total number of initiated flower primordia was counted.

For nondestructive plastochron measurements, the two youngest open flowers were removed on freshly bolted plants, leaving the pedicels as markers. Six days later, the total number of siliques and open flowers above the two removed flowers was counted.

To measure the rate of leaf initiation, plants were grown in short days, and the number of leaves visible by eye was counted at the indicated times.

The length of the basalmost five internodes was measured at maturity using a ruler. To determine cell length in the internodes, epidermal peels were stained with 0.1% toluidine blue and observed under a microscope.

### Positional Cloning

To identify the *SLOMO* locus, the wild-type *SLOMO* allele from the Col-0 accession was backcrossed twice into the *slomo-1* mutant in *Ler*. Recombination breakpoints were mapped in the resulting F2 using markers

designed on the basis of published information (Jander et al., 2002). Information on markers used is given in Supplemental Table 1 online.

### Molecular Cloning

Transgene construction was performed using standard techniques. Details on individual constructs are provided in Supplemental Methods online.

### Yeast Two-Hybrid Assay

The *SLOMO* coding region was cloned into plasmid pEG202 as a *Bam*HI fragment from pDL32. Screening for interacting proteins was performed as described by Grebe et al. (2000) using a library prepared from inflorescences and young siliques.

### In Situ Hybridization and Microscopy

In situ hybridization using an anti-histone H4 riboprobe was performed as described previously (Dinneny et al., 2004). GUS staining and scanning electron microscopy were performed as previously described (Schoof et al., 2000). The S-phase index was determined by relating the number of H4-positive cells in longitudinal sections of the inflorescence meristem to the total cell number as calculated from the area used for counting and the average cell area. The plastochron ratio was determined by measuring the distances between the center of the inflorescence meristem and the centers of the five youngest flower primordia and averaging over the four resultant individual ratios per plant.

YFP fluorescence was observed using a Zeiss 510 Meta confocal laser scanning microscope.

### PCR and RT-PCR

Details on oligonucleotides used for PCR-based genotyping are given in Supplemental Table 2 online.

For RT-PCR, total RNA was isolated from pooled inflorescences of *Col-0* and *slomo-3* plants using the Qiagen Plant RNeasy Mini Kit according to the manufacturer's instructions. Reverse transcription was performed using an oligo(dT) primer and SuperScript III reverse transcriptase (Invitrogen) according to the manufacturer's instructions. PCR products were visualized after agarose-gel electrophoresis using ethidium bromide staining. Details of oligonucleotides used for the subsequent PCRs are given in Supplemental Table 2 online.

### IAA Measurements

Inflorescence meristems of plants with fewer than 10 open flowers were dissected under a high-magnification stereomicroscope to leave only the youngest four to six floral meristems attached. The topmost 400 to 500  $\mu$ m of the remaining shoot was frozen in liquid nitrogen. For each sample, apices from 20 plants were pooled. The meristems were freeze-dried over night and their dry weight recorded using a Sartorius ME5-0CE microbalance. Roots of 20 seedlings were dissected and pooled per sample and freeze-dried over night. It was not possible to measure the dry weight of the roots; therefore, the values were expressed as pg IAA per root.

Lyophilized *Arabidopsis thaliana* tissues were ground in 500  $\mu$ L methanol prechilled at  $-20^{\circ}\text{C}$ . The samples were extracted for 1 h at  $4^{\circ}\text{C}$  under continuous shaking. As an internal standard,  $d_2$ -IAA (100 pg for inflorescence meristems and 20 pg for roots; Sigma-Aldrich) was added. After centrifugation (10,000g, 5 min), the supernatant was collected and passed through a 20- $\mu$ m filter (RESERVOIR-2 FRITS; Varian). The precipitate was extracted again with methanol for 10 min, centrifuged, and

filtered as described above. The combined filtrates were concentrated in vacuo, resuspended in 20  $\mu$ L of water containing 1% acetic acid, and injected into liquid chromatography (1200 series; Agilent)-electrospray ionization-tandem mass spectrometry (MS/MS; 6410 Triple Quad LC/MS; Agilent) equipped with a ZORBAX Eclipse XDB-C18 column (Agilent). A binary solvent system was used consisting of water containing 0.01% acetic acid as solvent A and acetonitrile containing 0.05% acetic acid as solvent B. Separations were performed using an isocratic elution with 15% solvent B at a flow rate of 0.2 mL/min. The retention time of IAA and  $d_2$ -IAA was 8.8 min. The MS/MS conditions were as follows: gas temp,  $300^{\circ}\text{C}$ ; gas flow, 9 L/min; nebulizer, 30 p.s.i.; capillary, 4000 V; fragmentor, 110; collision energy, 18; MS/MS transition ( $m/z$ ): 176/130 (unlabeled IAA), and 178/132 ( $d_2$ -IAA). The levels of IAA were calculated by MassHunter workstation software (Agilent).

### Auxin Transport Assay

Auxin transport assays were performed as described (Bennett et al., 2006), with the following slight modifications. Stem segments (18 mm long) excised from the most basal cauline internodes were incubated for 18 h in  $1\times$  *Arabidopsis* salts medium (ATS) containing 1% sucrose and radiolabeled IAA (1  $\mu$ M). The amount of transported radiolabel was quantified by scintillation counting (Top CountNXT; Packard Biosciences). Plants were cultivated in the greenhouse under long-day conditions with additional artificial light when needed. Six-week-old plants were used for analysis.

### Statistical Analysis

Comparisons of trait means were performed using Student's *t* test in SigmaPlot 10, with Bonferroni correction as appropriate.

### Accession Numbers

Sequence data from this article can be found in the GenBank/EMBL data libraries. The GenBank accession number for *SLOMO* mRNA is NM\_119475 and U60981 for *ASK1* mRNA. The Arabidopsis Genome Initiative locus identifier for *SLOMO* is At4g33210 and At1g75950 for *ASK1*. For the alignment in Supplemental Figure 3, the following sequences were used: At *SLOMO*, *Arabidopsis thaliana* (GenBank Q9SMY8); SI *SLOMO*, *Solanum lycopersicon* (Sol Genomics Network, sgn.cornell.edu, CU457764\_7.1); Vv *SLOMO*, *Vitis vinifera* (Genbank CAO43884); Os *SLOMO*, *Oryza sativa* (Genbank ABB47515); and Pp *SLOMO*, *Physcomitrella patens* (Genbank XP\_001756573).

### Supplemental Data

The following materials are available in the online version of this article.

**Supplemental Figure 1.** Whole-Plant Phenotypes and Plastochron Measurements of *slomo* Mutants.

**Supplemental Figure 2.** Molecular Nature of *slomo* Mutant Alleles.

**Supplemental Figure 3.** Sequence Alignment of *SLOMO* and Related Proteins from Other Plant Species.

**Supplemental Figure 4.** *slomo* Mutants Show Normal Auxin Sensitivity but Form More Lateral Roots and Longer Hypocotyls.

**Supplemental Figure 5.** The Pattern and Levels of *ProDR5* Promoter Activity Are Unchanged in *slomo* Mutants.

**Supplemental Figure 6.** Genetic Interactions between *SLOMO* and *miR156*.

**Supplemental Table 1.** Markers Used for Mapping the *SLOMO* Gene.

**Supplemental Table 2.** Oligonucleotides for PCR Genotyping and RT-PCR.

**Supplemental Methods.**

**Supplemental References.**

## ACKNOWLEDGMENTS

We thank Jia-Wei Wang, Detlef Weigel, Klaus Palme, Dolf Weijers, Yunde Zhao, the SALK Institute, and the Nottingham Arabidopsis Stock Centre for providing seeds. We are grateful to Isabel Bäurle and members of the Lenhard group for critical reading of the manuscript and helpful discussion. This work was supported by the Biotechnology and Biological Sciences Research Council through a David Phillips Fellowship to M.L., an ERA-NET Plant Genomics grant to O.L., and a research fund from RIKEN Plant Science Center to S.Y.

Received September 18, 2009; revised January 13, 2010; accepted January 25, 2010; published February 5, 2010.

## REFERENCES

- Anastasiou, E., Kenz, S., Gerstung, M., MacLean, D., Timmer, J., Fleck, C., and Lenhard, M. (2007). Control of plant organ size by KLUH/CYP78A5-dependent intercellular signalling. *Dev. Cell* **13**: 843–856.
- Bayer, E.M., Smith, R.S., Mandel, T., Nakayama, N., Sauer, M., Prusinkiewicz, P., and Kuhlemeier, C. (2009). Integration of transport-based models for phyllotaxis and midvein formation. *Genes Dev.* **23**: 373–384.
- Bennett, T., Sieberer, T., Willett, B., Booker, J., Luschnig, C., and Leyser, O. (2006). The Arabidopsis MAX pathway controls shoot branching by regulating auxin transport. *Curr. Biol.* **16**: 553–563.
- Chaudhury, A., Letham, S., Craig, S., and Dennis, E.S. (1993). *amp1*: A mutant with high cytokinin levels and altered embryonic pattern, faster vegetative growth, constitutive photomorphogenesis and precocious flowering. *Plant J.* **4**: 907–916.
- Christensen, S.K., Dagenais, N., Chory, J., and Weigel, D. (2000). Regulation of auxin response by the protein kinase PINOID. *Cell* **100**: 469–478.
- Cole, M., Chandler, J., Weijers, D., Jacobs, B., Comelli, P., and Werr, W. (2009). DORNROSCHEN is a direct target of the auxin response factor MONOPTEROS in the Arabidopsis embryo. *Development* **136**: 1643–1651.
- de Reuille, P.B., Bohn-Courseau, I., Ljung, K., Morin, H., Carraro, N., Godin, C., and Traas, J. (2006). Computer simulations reveal properties of the cell-cell signaling network at the shoot apex in Arabidopsis. *Proc. Natl. Acad. Sci. USA* **103**: 1627–1632.
- Dinneny, J.R., Yadegari, R., Fischer, R.L., Yanofsky, M.F., and Weigel, D. (2004). The role of JAGGED in shaping lateral organs. *Development* **131**: 1101–1110.
- Douady, S., and Couder, Y. (1996). Phyllotaxis as a dynamical self organizing process. *J. Theor. Biol.* **178**: 255–312.
- Fletcher, J.C., Brand, U., Running, M.P., Simon, R., and Meyerowitz, E.M. (1999). Signaling of cell fate decisions by CLAVATA3 in Arabidopsis shoot meristems. *Science* **283**: 1911–1914.
- Friml, J., et al. (2004). A PINOID-dependent binary switch in apical-basal PIN polar targeting directs auxin efflux. *Science* **306**: 862–865.
- Galweiler, L., Guan, C., Muller, A., Wisman, E., Mendgen, K., Yephremov, A., and Palme, K. (1998). Regulation of polar auxin transport by AtPIN1 in Arabidopsis vascular tissue. *Science* **282**: 2226–2230.
- Geier, F., Lohmann, J.U., Gerstung, M., Maier, A.T., Timmer, J., and Fleck, C. (2008). A quantitative and dynamic model for plant stem cell regulation. *PLoS One* **3**: e3553.
- Grebe, M., Gadea, J., Steinmann, T., Kientz, M., Rahfeld, J.U., Salchert, K., Koncz, C., and Jurgens, G. (2000). A conserved domain of the Arabidopsis GNOM protein mediates subunit interaction and cyclophilin 5 binding. *Plant Cell* **12**: 343–356.
- Grigg, S.P., Canales, C., Hay, A., and Tsiantis, M. (2005). SERRATE coordinates shoot meristem function and leaf axial patterning in Arabidopsis. *Nature* **437**: 1022–1026.
- Hardtke, C.S., and Berleth, T. (1998). The Arabidopsis gene MONOPTEROS encodes a transcription factor mediating embryo axis formation and vascular development. *EMBO J.* **17**: 1405–1411.
- Helliwell, C.A., Chin-Atkins, A.N., Wilson, I.W., Chapple, R., Dennis, E.S., and Chaudhury, A. (2001). The Arabidopsis AMP1 gene encodes a putative glutamate carboxypeptidase. *Plant Cell* **13**: 2115–2125.
- Hofmeister, W. (1868). Allgemeine Morphologie der Gewächse. In *Handbuch der Physiologischen Botanik*, W. Hofmeister, ed (Leipzig, Germany: W. Engelmann), pp. 405–664.
- Jander, G., Norris, S.R., Rounsley, S.D., Bush, D.F., Levin, I.M., and Last, R.L. (2002). Arabidopsis map-based cloning in the post-genome era. *Plant Physiol.* **129**: 440–450.
- Jensen, P.J., Hangarter, R.P., and Estelle, M. (1998). Auxin transport is required for hypocotyl elongation in light-grown but not dark-grown Arabidopsis. *Plant Physiol.* **116**: 455–462.
- Jonsson, H., Heisler, M.G., Shapiro, B.E., Meyerowitz, E.M., and Mjolsness, E. (2006). An auxin-driven polarized transport model for phyllotaxis. *Proc. Natl. Acad. Sci. USA* **103**: 1633–1638.
- Kawakatsu, T., Itoh, J., Miyoshi, K., Kurata, N., Alvarez, N., Veit, B., and Nagato, Y. (2006). PLASTOCHRON2 regulates leaf initiation and maturation in rice. *Plant Cell* **18**: 612–625.
- Kawakatsu, T., et al. (2009). PLASTOCHRON3/GOLIATH encodes a glutamate carboxypeptidase required for proper development in rice. *Plant J.* **58**: 1028–1040.
- Kuhlemeier, C. (2007). Phyllotaxis. *Trends Plant Sci.* **12**: 143–150.
- Lee, B.H., Johnston, R., Yang, Y., Gallavotti, A., Kojima, M., Travencolo, B.A., Costa Lda, F., Sakakibara, H., and Jackson, D. (2009). Studies of aberrant phyllotaxy1 mutants of maize indicate complex interactions between auxin and cytokinin signaling in the shoot apical meristem. *Plant Physiol.* **150**: 205–216.
- Lenhard, M., and Laux, T. (2003). Stem cell homeostasis in the Arabidopsis shoot meristem is regulated by intercellular movement of CLAVATA3 and its sequestration by CLAVATA1. *Development* **130**: 3163–3173.
- Ljung, K., Bhalerao, R.P., and Sandberg, G. (2001). Sites and homeostatic control of auxin biosynthesis in Arabidopsis during vegetative growth. *Plant J.* **28**: 465–474.
- Michniewicz, M., et al. (2007). Antagonistic regulation of PIN phosphorylation by PP2A and PINOID directs auxin flux. *Cell* **130**: 1044–1056.
- Miyoshi, K., Ahn, B.O., Kawakatsu, T., Ito, Y., Itoh, J., Nagato, Y., and Kurata, N. (2004). PLASTOCHRON1, a timekeeper of leaf initiation in rice, encodes cytochrome P450. *Proc. Natl. Acad. Sci. USA* **101**: 875–880.
- Mordhorst, A.P., Voerman, K.J., Hartog, M.V., Meijer, E.A., van Went, J., Koornneef, M., and de Vries, S.C. (1998). Somatic embryogenesis in *Arabidopsis thaliana* is facilitated by mutations in genes repressing meristematic cell divisions. *Genetics* **149**: 549–563.
- Okada, K., Ueda, J., Komaki, M.K., Bell, C.J., and Shimura, Y. (1991).

- Requirement of the auxin polar transport system in early stages of *Arabidopsis* floral bud formation. *Plant Cell* **3**: 677–684.
- Reinhardt, D., Pesce, E.R., Stieger, P., Mandel, T., Baltensperger, K., Bennett, M., Traas, J., Friml, J., and Kuhlemeier, C.** (2003). Regulation of phyllotaxis by polar auxin transport. *Nature* **426**: 255–260.
- Richards, F.J.** (1951). Phyllotaxis: Its quantitative expression and relation to growth in the apex. *Philos. Trans. R. Soc. Lond. B Biol. Sci.* **235**: 509–564.
- Schoof, H., Lenhard, M., Haecker, A., Mayer, K.F., Jurgens, G., and Laux, T.** (2000). The stem cell population of *Arabidopsis* shoot meristems is maintained by a regulatory loop between the *CLAVATA* and *WUSCHEL* genes. *Cell* **100**: 635–644.
- Schwab, R., Palatnik, J.F., Riederer, M., Schommer, C., Schmid, M., and Weigel, D.** (2005). Specific effects of microRNAs on the plant transcriptome. *Dev. Cell* **8**: 517–527.
- Smith, R.S., Guyomarc'h, S., Mandel, T., Reinhardt, D., Kuhlemeier, C., and Prusinkiewicz, P.** (2006b). A plausible model of phyllotaxis. *Proc. Natl. Acad. Sci. USA* **103**: 1301–1306.
- Smith, R.S., Kuhlemeier, C., and Prusinkiewicz, P.** (2006a). Inhibition fields for phyllotactic pattern formation: a simulation study. *Can. J. Bot.* **84**: 1635–1649.
- Steeves, T.A., and Sussex, I.M.** (1989). *Patterns in Plant Development*. (Cambridge, UK: Cambridge University Press).
- Stoma, S., Lucas, M., Chopard, J., Schaedel, M., Traas, J., and Godin, C.** (2008). Flux-based transport enhancement as a plausible unifying mechanism for auxin transport in meristem development. *PLOS Comput. Biol.* **4**: e1000207.
- Wang, J.W., Schwab, R., Czech, B., Mica, E., and Weigel, D.** (2008). Dual effects of miR156-targeted SPL genes and CYP78A5/KLUH on plastochron length and organ size in *Arabidopsis thaliana*. *Plant Cell* **20**: 1231–1243.
- Werner, T., Motyka, V., Laucou, V., Smets, R., Van Onckelen, H., and Schmülling, T.** (2003). Cytokinin-deficient transgenic *Arabidopsis* plants show multiple developmental alterations indicating opposite functions of cytokinins in the regulation of shoot and root meristem activity. *Plant Cell* **15**: 2532–2550.
- Werner, T., Motyka, V., Strnad, M., and Schmülling, T.** (2001). Regulation of plant growth by cytokinin. *Proc. Natl. Acad. Sci. USA* **98**: 10487–10492.